CHALMERS | UNIVERSITY OF GOTHENBURG

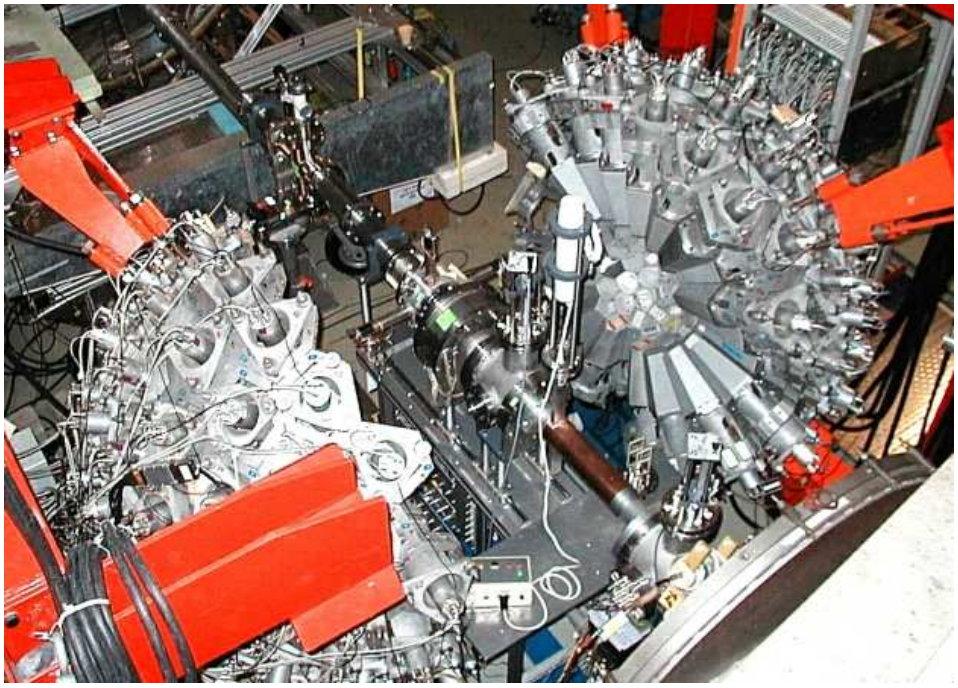

Calibration Detector for Crystal Ball

Thesis for the degree of Bachelor of Science

Thomas Axelsson, Vedad Babic, Per M Hansson,
Johannes Laurell Håkansson, Nikita S Kudelkin,
Niklas Rosholm

Department of Fundamental Physics
Division of Subatomic Physics
CHALMERS UNIVERSITY OF TECHNOLOGY
UNIVERSITY OF GOTHENBURG
Gothenburg, Sweden, 2012

Bachelor Thesis No. FUFX02-12-02

Calibration Detector for Crystal Ball.
Thomas Axelsson[a], Vedad Babic[b], Per M Hansson[c], Johannes Laurell Håkansson[d], Nikita S Kudelkin[e], Niklas Rosholm[f]

Email:
[a]axelthom@student.chalmers.se
[b]vedadb@student.chalmers.se
[c]pehan@student.chalmers.se
[d]johhaka@student.chalmers.se
[e]kudelkin@student.chalmers.se
[f]niklasr@student.chalmers.se

FUFX02 - Bachelor thesis at Fundamental Physics
Bachelor Thesis No. FUFX02-12-02

Supervisor: Andreas Heinz
Co-Supervisors: Håkan Johansson, Ronja Thies
Examiners: Christian Forssén, Ann-Marie Pendrill

Department of Fundamental Physics
Chalmers University of Technology
SE-412 96 Göteborg
Sweden
+46 (31) 772 1000

Printed by Chalmers Reproservice
Göteborg, Sweden 2012

Cover: Crystal Ball detector array located at GSI Helmholtz Centre for Heavy Ion Research in Darmstadt, Germany.[1]

[1] Official website of GSI. (2003). *The Crystal Ball Pictures*. Retrieved 5 June, 2012, from GSI Helmholtzzentrum für Schwerionenforschung GmbH. http://www-land.gsi.de/a_new_land/__public/documentation/detectors/crystal_ball/pictures/cb_opened_y2000.jpg

Abstract

Crystal Ball is a detector which can be used for detection of high energy protons, but this task requires a potentially tedious and expensive process of calibration. In this study, a test setup using a single NaI crystal from the Crystal Ball was considered to investigate the possibility of using cosmic muons to calibrate the Crystal Ball. The study was performed by simulating the process using the Geant4 toolkit. A program was written to simulate the passage of cosmic muons and protons through the Crystal Ball crystal, record the deposited energy and correlate these to each other. A setup which can be used for finding the correlation experimentally is proposed. Using the results from the experiment, it is possible to calibrate all crystals in Crystal Ball using cosmic muons.

This page is intentionally left blank.

Acknowledgements

This project could not have been realised without the help of many people.

First of all we would like to thank our supervisor Andreas Heinz, whose untiring support, limitless patience and infectious good spirits during the project served as an inspiration for us all. He was always available for interesting discussions and any mail sent would get a reply in a few hours regardless of the time of day.

We would also like to thank Håkan Johansson. His skills as a computer wizard was of great help when we were getting acquainted with the software. His enthusiasm and knack of getting to the root of a problem also proved to be a great asset when we ran into trouble.

Furthermore we would like to thank Ronja Thies, whose previous experience of working with the Crystal Ball was of great help.

Last, but not least, we would also like to thank Simon Lindberg for insightful comments and proof-reading our thesis.

This page is intentionally left blank.

Contents

This page is intentionally left blank.

1 Introduction

1.1 Background

The goal of research within the field of subatomic physics is to gain knowledge about the properties and structure of nuclei. This is mainly accomplished through experiments where results from collisions between particles are analyzed.

GSI in Darmstadt, Germany, is one site where this area of physics is explored. Research is conducted using equipment consisting of particle accelerators, detectors etc. One of the detectors at GSI, which is the focus of this project, is the Crystal Ball.

Crystal Ball is a detector array which serves as a 4-π-spectrometer. This means that the array encompasses an entire sphere around the target, a solid angle of 4π steradians. The detector consists of 162 sodium iodide (NaI) crystals put closely together to form a sphere with an inner radius of 25 cm and an outer radius of 45 cm, see Figure 1.

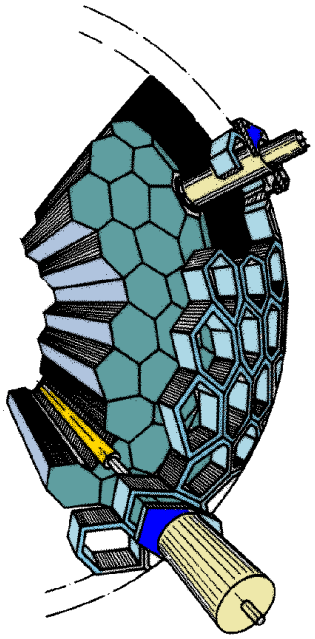

Figure 1: A closer look at a section of the Crystal Ball's detector array [1].

When conducting an experiment, one places a target in the centre of the Crystal Ball. This target can be, for example, made of plastic, carbon or lead. A beam of unstable particles, which are created in nuclear reactions at a production target, collides with the experimental target nuclei. Due to kinematics most reaction products move in the forward direction but some of the lighter particles scatter at larger angles. To detect these particles and photons, Crystal Ball is used.

Being initially optimized for detection of low energy γ-rays ($1 - 3\,\mathrm{MeV}$), the Crystal Ball is now also used for detection of high energy protons (several hundred MeV). To make good use of it for detection of high-energy protons it needs a proper calibration.

A problem arises in the question of how to calibrate all crystals of Crystal Ball. Since it is both expensive and burdensome to calibrate all crystals one by one with a proton beam, there is a need for a freely available source with a well-defined energy spectrum to be used for calibration. A candidate for such a source are cosmic muons, denoted by μ. These particles are created in the atmosphere as a result of a cascade of reactions that follow from the interaction of cosmic radiation with the nuclei of air molecules, see section 2.3 for more information.

To make use of the muons, it is sufficient to calibrate one crystal with the proton beam and correlate this to the energy deposit in the crystal from the muons. This can be done because the energy spectrum of the muons and their angular distribution are well known [12]. This way they can be used to calibrate the other crystals for detection of high energy protons.

Since the energy deposited by muons depends on the length traversed through crystal, it is desirable to track the path through the crystal taken by the muons. In the Crystal Ball, several crystals "fire off" when a particle passes through them, enabling path tracking. For a single crystal there will not be any crystals nearby to fill this role. Therefore one uses plastic scintillators, which are cheap and easy to handle, to track the path length. See section 2.1 for more information on scintillators.

1.2 Purpose and objectives

The purpose of the project is to develop a way of calibrating a Crystal Ball crystal with cosmic muons. This is done by designing a suitable detector setup for the calibration of a single Crystal Ball crystal against protons. The results will in turn be used to calibrate all detectors of Crystal Ball with muons on the basis of Monte Carlo simulations.

The actual calibration procedure was not executed within this project. The purpose of the project was to provide simulations and guidelines for an upcoming calibration experiment intended to be accomplished in at most three days.

2 Theory

This section will introduce the theory behind the measurement equipment and materials involved, as well as the particles that will be used for the calibration.

2.1 Scintillators

A scintillator is a material that de-excites by emission of light when atoms in it have been excited by ionizing radiation, a luminescence process called scintillation. There are several different types of scintillators with different properties. The ones relevant in this project however are plastic scintillators and sodium iodide crystals doped with thallium (Tl).

Sodium iodide is used as a scintillator material because of its good stopping power and energy resolution [6]. The resolution for stopped protons in a NaI crystal is 2% or less. For punchthrough protons the resolution is around 5% [21]. The reason for using plastic scintillators is for convenience as plastic is cheap, easy to manufacture, shape and handle. Moreover, plastic scintillators give a very fast response [6].

2.1.1 Inorganic scintillators

In a crystal of sodium iodide (NaI), which is an inorganic material, the scintillation occurs due to the crystal structure of the lattice. The bandgap between the valence and conduction band is large, making photon emission an inefficient way of de-exciting the electrons of the material. Due to this fact one adds an activator (in our case thallium), an impurity, to the crystal to add extra energy bands in the forbidden zone between valence and conduction band. The activator is added in trace amounts, meaning that the overall energy structure of the crystal remains unchanged, while the band structure at the lattice point where the activator is being placed, is changed. The activator is chosen such that it allows photons with lower energies, lying in the visible range of light, to be emitted with higher probability.

2.1.2 Organic scintillators

In contrast to inorganic scintillators, the scintillation of organic scintillators does not appear due to the lattice structure of a crystal, but rather it originates from the fluorescence mechanism of single molecules. The fluorescence arises from transitions in the energy levels of these molecules and is independent of the state in which the molecules are in, be it a gaseous mix or a solid. The plastic scintillators used in this project is an example of a type of organic scintillator.

2.1.3 Measurements and equipment

To make use of a scintillator one needs to connect photomultiplier tubes (PMTs) to it. These together with some electronic equipment constitute a scintillation counter. This makes it possible to detect the scintillation photons, which are in turn transformed into an electric signal with a certain amplitude.

2.2 Minimum ionizing particles

Energy loss in a material can be of different types, such as ionization, radiative processes and others. Which of these processes that dominate the total energy loss depends on the energy of the incoming particle as well as the material used. If the energy of the incoming particle is within a specific interval of energy the energy loss per unit path length goes to a minimum. Particles with energy within this interval are called minimum ionizing particles [8].

At energies up to about 100 GeV, the deposited energy in the crystal is described by the Bethe-Bloch formula [10]. This is an empirical formula expressing the energy loss per unit length, due to excitation and ionization, of a charged particle travelling through matter.

At energies well above 100 GeV radiative processes will become the main factor for determining deposited energy, as opposed to ionization. Cosmic muons have energies well within the range where muons can be treated as minimum ionizing particles [9]. Figure 2 shows an example of the region of minimum ionization for antimuons in copper.

A minimum ionizing particle's energy loss, in a material, is only dependent on the thickness of the material passed, regardless of the initial energy of the particles. The stopping power in the region $0.1 - 50\,\text{GeV}$ varies very weakly with the energy of the muons ($1.5 - 2.1\,\text{MeVcm}^2\text{g}^{-1}$), see Figure 2. Therefore a broad energy distribution may result in a well-defined energy deposit in a detector. Hence it can be used for calibration.

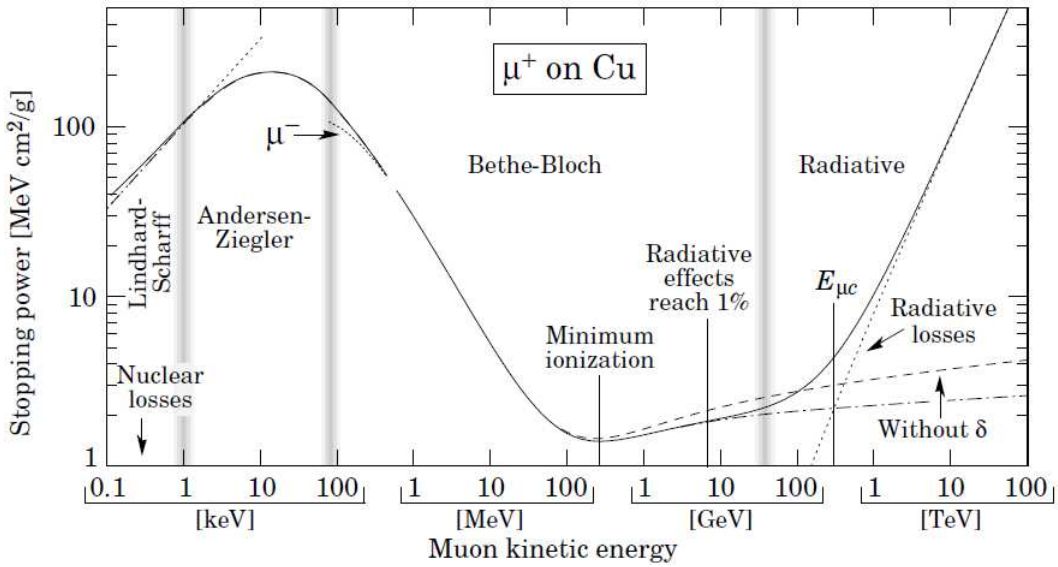

Figure 2: Stopping power for μ^+ in Cu as a function of the muon kinetic energy [10].

2.3 Muons

A muon is an unstable subatomic particle with a charge equal to that of an electron and a mass of $105.7\,\text{MeV/c}^2$, which corresponds to 206.8 times the mass of an electron [7]. Most muons on earth are created in the upper atmosphere, usually through the process described below.

As high-energy nuclei from cosmic rays interact with atmospheric nuclei, kaons, denoted by K, and pions, denoted by π, are produced. A negative pion decays to a muon and a muon-type antineutrino, with a mean lifetime of about 26 ns, and thus survives only a few meters on average. The muon created has a mean lifetime of 2.2 μs and decays to an electron, an electron-type antineutrino and a muon-type neutrino. The different reactions and decays are shown in equation (1).

$$\begin{aligned} A_{cr} + A_{air} &\rightarrow \pi^{\pm}, K^{\pm}, K^{0} \\ \pi^{-} &\rightarrow \mu^{-} + \bar{\nu}_{\mu} \\ \mu^{-} &\rightarrow e^{-} + \bar{\nu}_{e} + \nu_{\mu} \end{aligned} \tag{1}$$

The somewhat longer half-life of the muon is due to the fact that it decays by the weak force. The time dilation effect of special relativity results in a mean traveled distance that is sufficiently large so about 10 % of the muons reach sea level [14]. The muons generally travel in the same direction as the cosmic rays from which they originate.

The intensity of incoming muons at sea level depends on the incident zenith angle as well as the muon energy and this dependence has been measured. It is described by equation (2), where p_μ is the muon momentum in GeV/c, θ is the zenith angle and $I(0)$ is the intensity for vertical muons [13].

$$\log(I(\theta)) = a \ln^2 p_\mu + b \ln p_\mu + c \tag{2}$$

Equation (3) below is used to obtain the parameters a and b , where y means a or b respectively, while equation (4) is used to calclulate c, both using data from Table 1. These empirical relations describe the measured intensities for muons with an energy between $0.2 - 100\,\mathrm{GeV/c}$ [13], which corresponds to the energy region where muons can be treated as minimum ionizing particles [9].

$$y = p_1/(1/\theta + p_2\theta) + p_3 + p_4 \exp(-p_5\theta) \tag{3}$$

$$c = p_1\theta^2 + p_2\theta + p_3 + p_4 \exp(-p_5\theta) \tag{4}$$

	a	b	c
p_1	$-0.8816 \cdot 10^{-4}$	$+0.4169 \cdot 10^{-2}$	$-0.3516 \cdot 10^{-3}$
p_2	$-0.1117 \cdot 10^{-3}$	$-0.9891 \cdot 10^{-4}$	$+0.8861 \cdot 10^{-2}$
p_3	-0.1096	$+4.0395$	-2.5985
p_4	$-0.1966 \cdot 10^{-1}$	-4.3118	$-0.8745 \cdot 10^{-5}$
p_5	$+0.2040 \cdot 10^{-1}$	$-0.9235 \cdot 10^{-3}$	-0.1457

Table 1: Parameters for the equations (2), (3) and (4) [12].

2.4 Punchthrough of particles

As the Crystal Ball initially was not designed to detect high-energy protons, the crystals in the detector are not long enough to stop all the protons produced in the experiments.

Punchthrough describes the situation of a particle traveling through a material, ionizing it and losing only a part of its kinetic energy. Since the particle does not lose all of its kinetic energy, it will continue its path out of the material and thus 'punch through' the material, see the upper part of Figure 3.

The opposite process is total loss of kinetic energy, resulting in the incoming particle being stopped in the material. The particle never escapes the boundaries of the material as seen in the lower part of Figure 3.

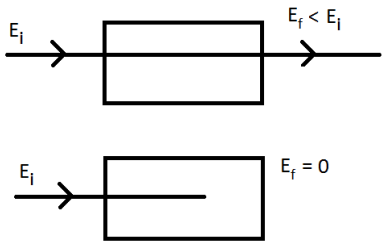

Figure 3: The upper figure demonstrates punchthrough while the lower figure demonstrates a particle being stopped. The initial and final energies, E_i and E_f, are the kinetic energies of the particles.

3 Method

3.1 Geant4

The test setup consists of one Crystal Ball detector and plastic scintillators. The latter are necessary to determine the trajectories of incoming muons. In the present study, simulations were conducted with version 9.4 of the Geant4 toolkit. Geant4 is an object oriented development framework developed at CERN (European Organization for Nuclear Research) for "simulating the passage of particles through matter", and was developed for making accurate simulations of particle detectors, but also has many applications in e.g. medicine and astrophysics [2]. The toolkit, based on the programming language C++, allows the user to define the geometry of a detector with different materials, and then simulate particles and track their interactions with the detector through a cornucopia of physics processes.

The Geant4 framework handles runs, events and the tracking of particles, all of which are available for the user to manipulate. Here, a run is a preset number of particles to be generated in the simulation, and an event is the simulation of a single particle. The tracking of a particle is handled in small steps, as it traverses the materials in the detector. The programmer can supply his own code to conduct a virtual experiment - from the geometry and materials in the detector, to the number of simulated particles and particle direction. There is also a possibility to manipulate data output after need [3].

Geant4 simulates electromagnetic processes, as well as hadronic interactions for high- and low-energy physics and uses Monte Carlo methods for calculating the probability of certain events occurring, see Table 2. The Monte Carlo engine of Geant4 handles probabilities for the occurrence of physics processes and, as is the case with all statistical processes, the error results from such simulations. The validity and accuracy of Geant4 simulations of electromagnetic processes has been proven in a number of studies [4][5].

3.2 Software for simulations

To study basic physics processes with muons and protons in a scintillating material, a program was written within the Geant4 framework that generated particles of a user defined energy with momentum along the symmetry axis of a cylinder with length 20.0 cm and diameter 10.0 cm. See Figure 4 for an example of the visual output from the program.

To run simulations of an actual crystal from the Crystal Ball array together with plastic scintillators, another program was written that reads a scintillator setup from a user created data file. This program also employs a realistic angle- and energy distribution of muons, together with the geometry of a Crystal Ball crystal. All scintillators were simulated as having a thickness of 0.5 cm.

The Crystal Ball is made up of crystals of four different crystal shapes in order to build up a solid, hollow sphere, much like the pattern of hexagons and pentagons on a soccer ball. The measures for the crystal were obtained from GSI, and the shape called "D" is expected to be used for the calibration experiment. The crystal is defined by the points (6.80, 4.33), (0.0, 10.09), (-6.80, 4.33), (-6.80, -4.33), (0.0, -10.09), (6.80, -4.33) all measures in cm taken at a reference radius of 49.9 cm, see Figure 5. The shape is then spanned between an inner radius of 25 cm and

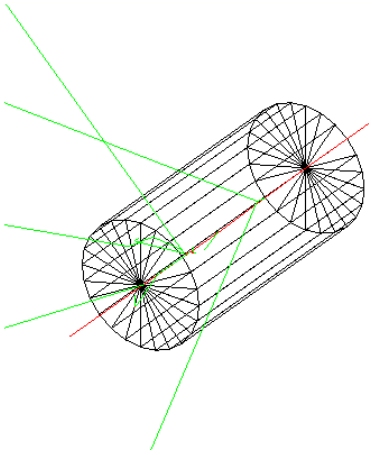

Figure 4: Visual output from the experimental setup in Geant4 - a muon traversing straight through the center of a NaI cylinder. The rays originating from the center are gamma photons created from the interaction between muon and crystal.

an outer radius of 45 cm. See Figure 6 for an example of visual output from the program and illustration of the crystal shape.

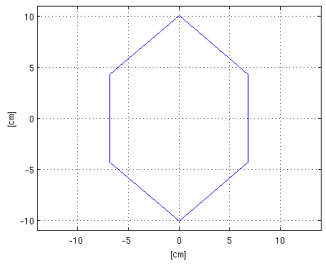

Figure 5: Profile of crystal shape ''D" used in simulations.

For every event the program saves the amount of energy that is deposited in the crystal, and in the scintillators, to enable a post hoc coincidence measurement. Data was collected and analyzed with the ROOT toolkit. ROOT is an object-oriented data analysis package designed to handle large data amounts typical for experiments in particle physics [16].

3.3 Simulated materials and processes

For the NaI crystal, data from Geant4's included NIST (National Institute of Standards and Technology) material database was used, while the material in the plastic scintillators were defined in Geant4 as a mix of H and C with a total density of $1.032\,\mathrm{g/cm^3}$, and a ratio between H:C of 10:9 [19]. The physics processes included in the simulations can be found in Table 2.

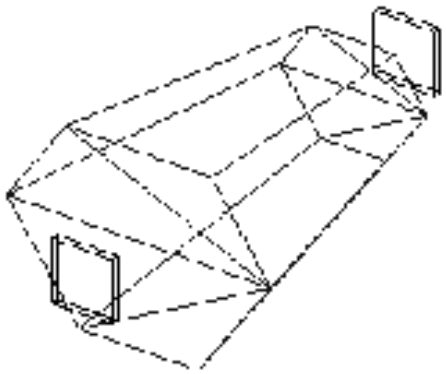

Figure 6: Visual output from the experimental setup in Geant4 - a crystal together with two plastic scintillators.

3.4 Simulated muon distribution

In order to achieve a realistic distribution of muons impinging on the crystal, a modified hemisphere was constructed around the crystal. Initially a position vector was randomized on the hemisphere with center in the origin, using uniformly randomized values of θ and ϕ in spherical coordinates.

$$\theta \in [0, \frac{\pi}{2}] \tag{5}$$

$$\phi \in [0, 2\pi] \tag{6}$$

This resulted in a position vector $\overrightarrow{v_p} = (x_p,y_p,z_p)$ with x_p, y_p and z_p given by equations (7)-(9), where R is the radius of the hemisphere.

$$x_p = R\cos\phi\sin\theta \tag{7}$$

$$y_p = R\sin\phi\sin\theta \tag{8}$$

$$z_p = R\cos\theta \tag{9}$$

An offset vector, $\overrightarrow{v_o}$, orthogonal to the position vector was obtained by deriving its coordinates with respect to θ. $\frac{\delta\overrightarrow{v_p}}{\delta\theta}$ was used since $\frac{\delta\overrightarrow{v_p}}{\delta\phi}$ is equal to zero at $\theta = 0$, and, thus, does not give us a uniform distribution.

The acquired offset vector was rotated by a randomized angle α around the position vector and its magnitude, r, was set by the the magnitude of the position vector times the square root of a randomized scalar between zero and one. This was done to achieve equal probability for each point on a disc tangential to the hemisphere.

Particle	Enabled processes
Gamma photons	
	Photoelectric effect
	Compton scattering
	Gamma conversion
Electrons/Positrons	
	Multiple scattering
	Ionisation
	Bremsstrahlung
	Annihilation
Muons	
	Multiple scattering
	Ionisation
	Bremsstrahlung
	Pair production
Protons	
	Multiple scattering
	Ionisation
	Bremsstrahlung
	Pair production
Alpha/He-3/Ions	
	Multiple scattering
	Ionisation

Table 2: Table of particles and associated physics processes included in the simulations.

$$m \in [0, 1] \tag{10}$$

$$r = R\sqrt{m} \tag{11}$$

$$\alpha \in [0, 2\pi] \tag{12}$$

The start position of the muon was set according to equation (13), see Figure 7, and the momentum direction of the muon was set to $-\overrightarrow{v_p}$.

$$\overrightarrow{v} = \overrightarrow{v_p} + \overrightarrow{v_o} \tag{13}$$

The modified hemisphere was tested to make sure that it provides a uniform distribution. This was done by placing ten detectors at the bottom of the half sphere as rings at different radii but all of which had the same surface area on the top. Simulations were made where the number of hits on each surface were acquired. In Table 3 the number of hits on each surface are given for a simulation of one million muons sent from the half sphere.

The distribution given by equation (2) was then implemented into the sphere. This was done by first randomizing values for θ and muon momentum in intervals appropriate for the simulation,

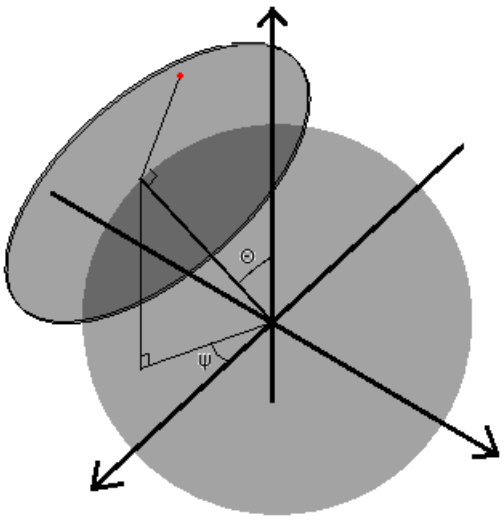

Figure 7: Visualisation of the modified hemisphere.

and using these values to calculate I as in equation (2). The result was then compared to a randomized test value between zero and the maximum value of I, and the particle was created if the test value was smaller than the value of I. If the test value was greater than I, then the values for θ, muon momentum and the test value were randomized again and the check redone. The cycle was repeated until the test value was smaller than I. This gave a proper setup for doing the simulations with the actual muon distribution. The distribution, as intensity plotted against zenith angle and muon momentum, is given in Figure 8.

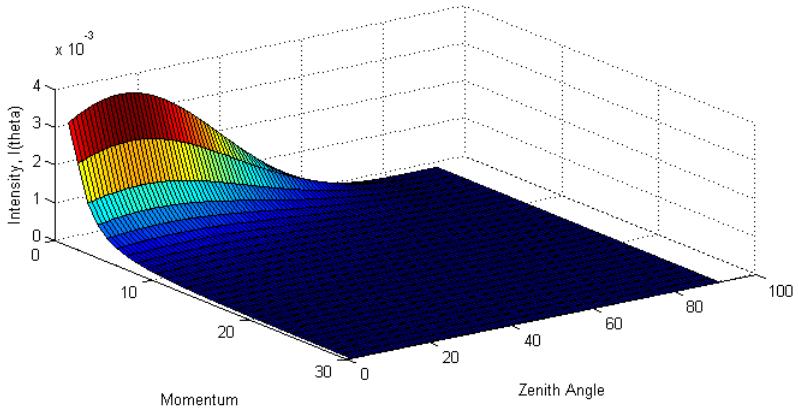

Figure 8: The muon distribution. Intensity of muons as a function of zenith angle, in °, and muon momentum, in GeV/c.

Hits per detector	
Detector 1	98860
Detector 2	100101
Detector 3	100280
Detector 4	99364
Detector 5	100284
Detector 6	100373
Detector 7	100421
Detector 8	100094
Detector 9	99922
Detector 10	100301

Table 3: Number of hits on each detector for 1 000 000 events from the hemisphere for uniform distribution.

3.5 Simulations of horizontal scintillators

The crystal will be held horizontal during calibration with protons of known energies and it is desired to use the same setup simultaneously for measuring energies deposited by cosmic muons. Then there are two main parameters to investigate: size and separation of the plastic scintillators used to track muons through the length of the crystal. In order to investigate how scintillator size and separation might affect measurement accuracy and measurement time for horizontal muons, a set of scintillator setups was created, see Figure 9. The muon flux is at its lowest at the horizontal, so it was decided that the scintillator at the narrow (front) end of the crystal should be made as large as the geometry allowed for, and this size was kept at a constant $5.5 \times 5.5\,\text{cm}$. The scintillator at the broader (back) end of the crystal was changed in size, and the sizes $5.5 \times 5.5\,\text{cm}$, $9.5 \times 9.5\,\text{cm}$, $13.5 \times 13.5\,\text{cm}$ and $17.5 \times 17.5\,\text{cm}$ were tested.

After initial analysis of the data it was decided to run further simulations on the scintillator setup with the most favorable geometry i.e. a setup that maximized the muon particle flux. The scintillator at the narrow (front) end of the crystal was chosen with a size of $5 \times 5\,\text{cm}$ and the scintillator at the broader (back) end of the crystal with a size of $13.7 \times 13.7\,\text{cm}$.

In order to investigate how the separation between the front- and back scintillators affected measurements, simulations were run where the scintillators' areas were kept constant at $5 \times 5\,\text{cm}$, while their separation was changed to 42 cm, 47 cm, 52 cm and 57 cm. See Figure 9 for a schematic view of the changes in separation and size. The back scintillators were placed with a distance of at least 0.5 cm from the simulated equipment, and with enough space to fit a PMT between one scintillator and the crystal.

To cut down on simulation time the simulations with horizontal scintillators were run with a modified muon distribution that only simulated particles coming from a zenith angle between 60° and 90°, i.e. candidates for actually traversing both scintillators. This saved a considerable amount of time, as the intensity for muons at higher angles are orders of magnitude lower than the vertical ones.

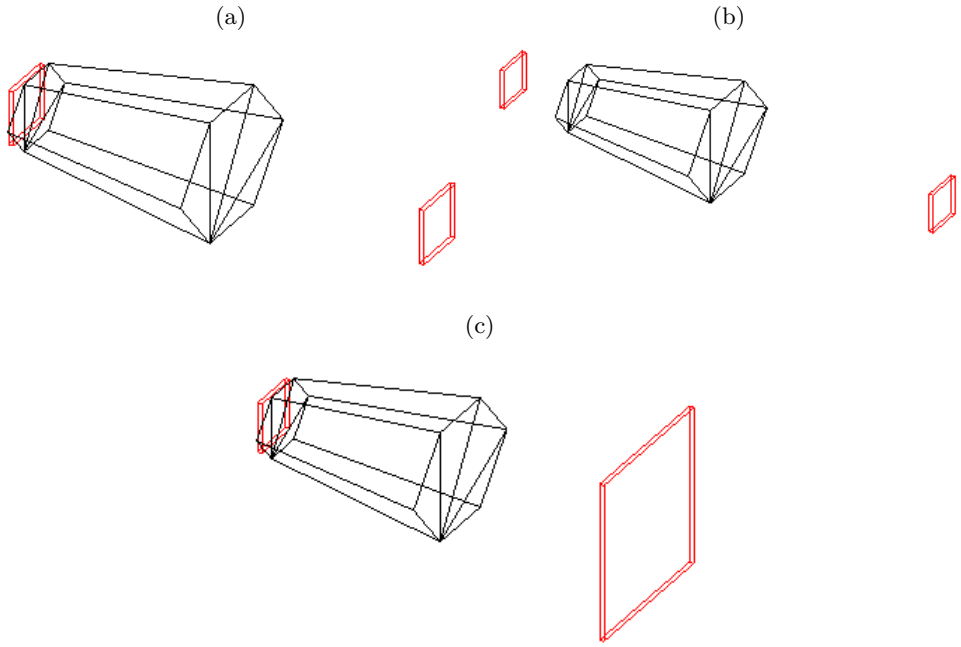

Figure 9: Extremes for scintillator size and placement in the simulations of horizontal detection: (a) closest to crystal and PM-tube, (b) furthest apart, (c) largest tested back scintillator.

3.6 Simulations of vertical scintillators

In order to determine how the size of the plastic scintillators affect the results – there should be a size beyond which no significant gains in resolutions are made – different setups were tested where the sizes and numbers of scintillators were changed, see Figure 10.

3.7 Estimation of muon particle flux

As there is a finite time in which to perform the calibration with the single detector and its associated plastic scintillators, an estimation of the muon particle flux through different scintillator configurations is needed. Suppose a certain setup gives a well-defined path length through the crystal. If the number of muons that pass through that configuration of scintillators is very low though, the time required to get enough muons for good statistics is impractical.

To estimate the muon particle flux through different scintillator configurations the theoretical flux through a simple scintillator setup was calculated, see subsection 3.8. Simulations were then run on that setup and the number of hits were compared with the theoretical value, which resulted in a correlation factor between the two.

For the simulation mentioned above, a total of $6 \cdot 10^7$ particles were shot, 6476 of them passing the two vertically placed detectors. With a calculated theoretical value, τ, of one muon passing the vertical setup every 423 seconds, the simulation represented the setup being bombarbed by muons for a duration of $\tau \cdot 6476 \approx 2.74 \cdot 10^6$ s.

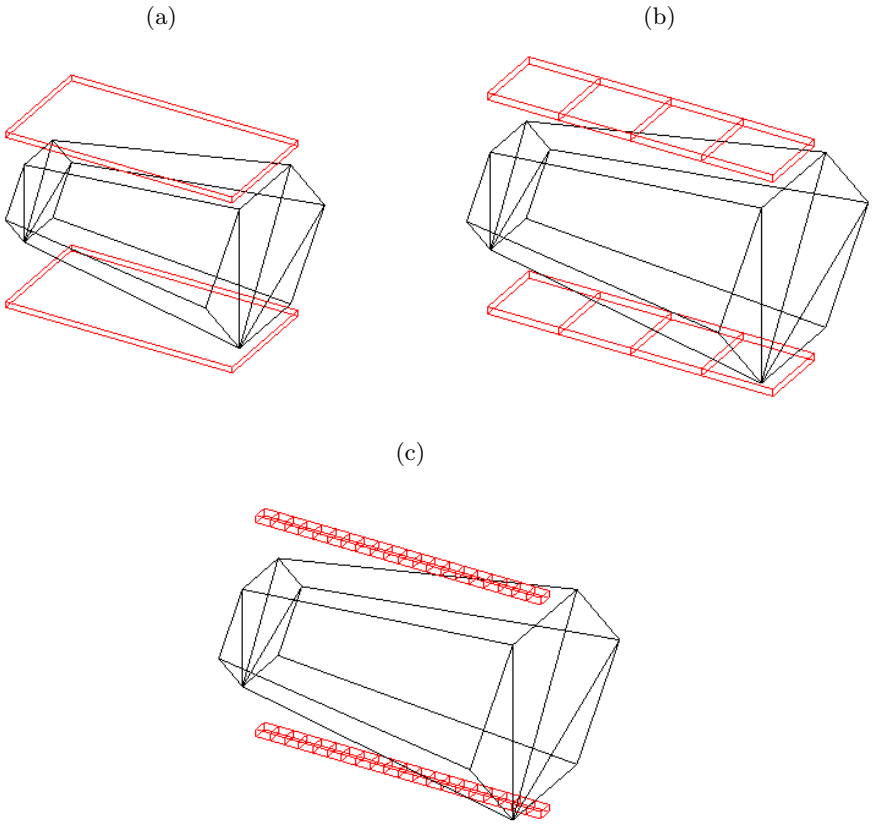

Figure 10: Some of the different setups used to detect vertical muons: two rows of (a) one $10 \times 20\,\text{cm}$ scintillator, (b) four $5 \times 5\,\text{cm}$ scintillators, (c) twenty $1 \times 1\,\text{cm}$ scintillators.

Also included in the same simulation was another pair of scintillators, this one horizontally placed. This was done in order to correlate the ordinary muon distribution with the modified distribution mentioned in subsection 3.5. The scintillator setup used in the simulation is shown in Figure 11.

3.8 Theoretical muon particle flux through a simple scintillator setup

The angular intensity of cosmic muons can be approximated using the following empirical relationship

$$I(\theta) \approx I(0)\cos^2\theta \tag{14}$$

where θ is the zenith angle and $I(0)$ the vertical intensity ($\theta = 0$) [13]. $I(\theta)$ is given in units of $\text{cm}^{-2}\text{s}^{-1}\text{sr}^{-1}$, which means that $I(\theta)$ is the number of particles passing through a certain area from a certain solid angle every second. The angular intensity is uniform with respect to ϕ.

To calculate the muon particle flux, J, through a scintillator one needs to integrate the angular intensity over the solid angle Ω, which the scintillator "sees".

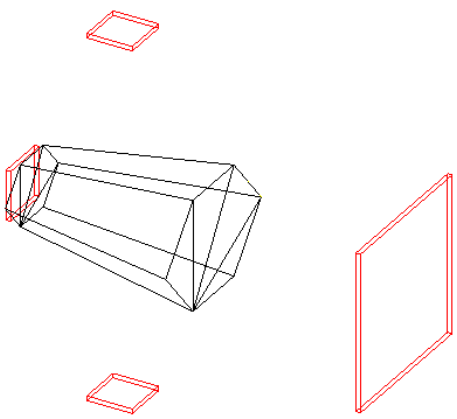

Figure 11: Setup used to obtain correlation factors between the real muon particle flux and the simulated.

$$J = \int I(\theta)\cos(\theta)\,\mathrm{d}\Omega \tag{15}$$

where the $\cos\theta$ term is due to the fact that the flux across a surface depends on the angle between the surface normal and the direction of the particles.

The vertical intensity $I(0)$ is calculated by using equation (2) and integrating the expression for $I(0)$ with respect to the momentum, $1\,\mathrm{GeV/c} \leq p_\mu \leq 30\,\mathrm{GeV/c}$. The values for the momentum chosen here are the ones used in section 3.4, also see Figure 8. Integration using MATLAB yields

$$\int_1^{30} I(0)\,\mathrm{d}p_\mu \approx 6.4 \cdot 10^{-3} cm^{-2} s^{-1} sr^{-1} \tag{16}$$

For a simple setup two square scintillators, of the same size, are placed, one above the other, at a fixed distance from each other. The muon particle flux through this setup is equal to the flux through the bottom scintillator over the solid angle the bottom scintillator "sees". To simplify the geometry the following two assumptions are made:

1. Each small area element of the scintillator "sees" the same solid angle as the one "seen" by the center of the detector.

2. The square scintillators are modeled as circular, having the same area.

The solid angle that the center of the bottom scintillator "sees" is now simply the solid angle subtended by a cone, see Figure 12.

$$\int_{cone} \mathrm{d}\Omega = \int_0^\theta \sin(\theta')\,\mathrm{d}\theta' \int_0^{2\pi} \mathrm{d}\phi \tag{17}$$

Combining equations (14), (15) and (17) yields a muon particle flux for this particular setup of

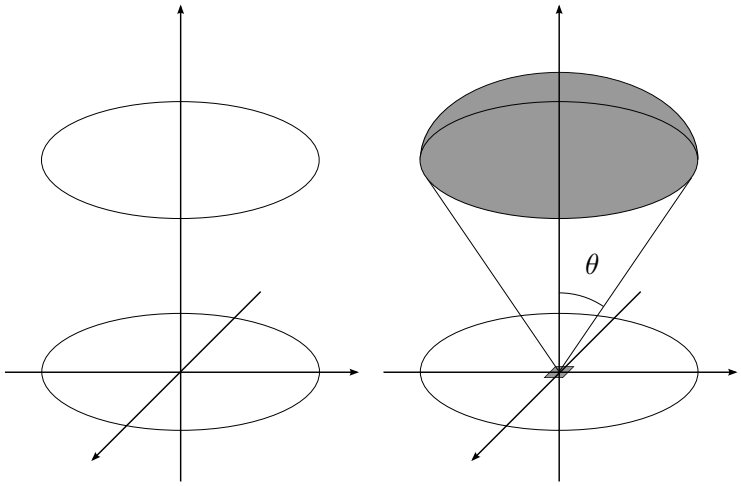

Figure 12: Left: A simple setup of two scintillators. Right: The solid angle "seen" by a small area element at the center of the bottom scintillator.

$$J \approx 2\pi \int_0^{\theta} (I(0)\cos^2\theta)\cos\theta\sin\theta\,\mathrm{d}\theta = \left(\frac{\pi}{2}\right) I(0)(1-\cos^4\theta) \tag{18}$$

where J is given in units of $\mathrm{cm}^{-2}\mathrm{s}^{-1}$. To get the total number of muons that passes through the scintillator every second one simply multiplies J by the area of the scintillator.

To illustrate, an example can be taken of a simple setup using square scintillators with a side length of 5 cm and a distance between the two of 41 cm. For this setup equation (18) yields an estimated total muon particle flux, $J_{tot} = 0.0024\,\mathrm{s}^{-1}$ i.e. one muon passes the two detectors every 423 seconds ($\tau = 423\,\mathrm{s}$).

4 Energy deposit in NaI for muons and protons

In this section the behaviour of muons and protons passing through sodium iodide were investigated. Simulations in this section were all run with a cylinder, composed of NaI, with a radius of 10 cm while the length was varied between 5 cm, 10 cm, 15 cm and 20 cm. The number of particles impinging was 10000 in all simulations. The incoming particles hit the crystal top surface perpendicular to it.

4.1 Muon behaviour

By impinging mono-energetic beams of muons into cylinders of fixed length one can find systematics in the deposited energy of the muons by varying these parameters. The deposited energy spectra that resulted from the simulation were fitted with Landau distributions.

When charged particles, in this case muons, traverse a thin layer of matter the deposited energy is centered around a most probable value, and positively skewed toward higher energies. This means that a Gaussian distribution with mean and variance is not suited for analysis of deposited energies. A curve that does fit these data well is the Landau distribution, with two parameters: most probable value, MPV, and a scale parameter, σ. A smaller σ gives a narrower peak. The most interesting parameter for this study is the most probable value along with its error. For an example of a curve fit to a Landau distribution, see Figure 13.

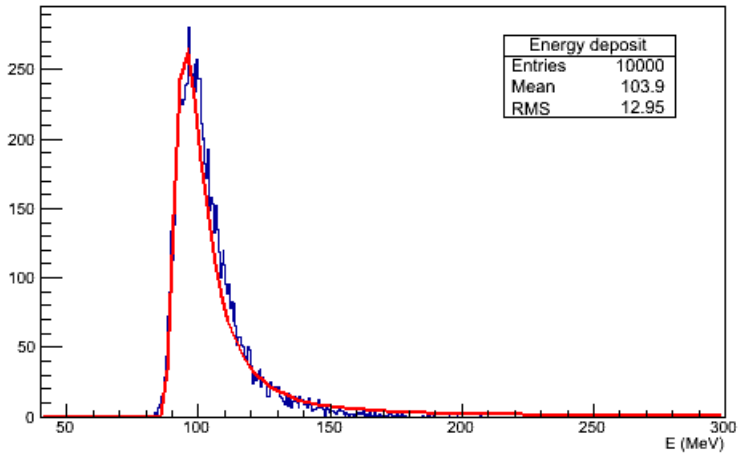

Figure 13: A Landau distribution fitted to data corresponding to the deposited energy of monoenergetic and monodirectional muons traversing a NaI-cylinder of length 20 cm. The muons have an kinetic energy of 1.0 GeV and traversed through the center of the cylinder. The σ value for the distribution is 3.50 MeV.

4.1.1 Energy and length dependence

By collecting the information for different lengths traveled through the crystal at different energies one finds a relation between the two. The results are plotted in Figure 14. Since muons in this case are minimum ionizing particles, see section 2.2, it is expected that their energy deposit is linearly dependent on the traversed length through the crystal.

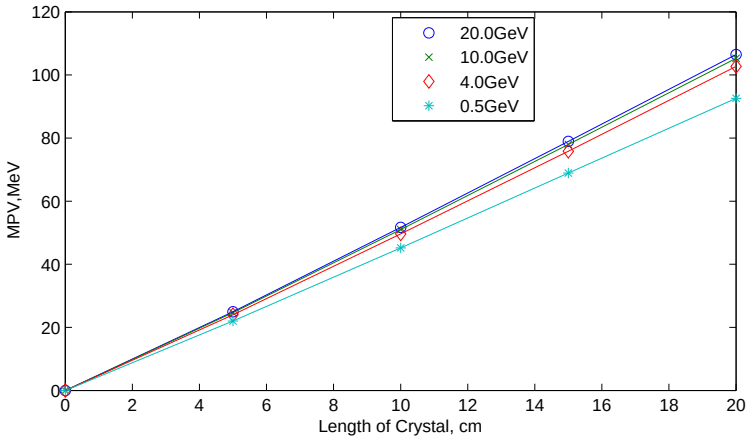

Figure 14: The most probable value (MPV) of deposited energy extracted from simulations where muons traversed the center of a NaI cylinder of varying length plotted against the cylinder length for different energies. The data is fitted to a Landau distribution, see Figure 13. The graph includes error-bars from the fit of the MPV, although too small to be seen by the naked eye.

To find the dependence of incoming energy to deposited energy, muons traversing the crystal with energies varying from 0.5 GeV up to 20 GeV were simulated. The results of those simulations are presented in Figure 15. One can clearly see that the energy deposited does not vary much with incoming energy between 4 GeV and 20 GeV ($3.6\% - 4.15\%$ relative backward error). Once again this is due to the particles being minimum ionizing.

4.1.2 Surface effects

There exist surface effects i.e. the deposited energy varies depending on where the muon hits the crystal, that is, if it is close to the surface or not. One can argue that, as the muons impinge closer to the surface the secondary particles created can scatter out of the cylinder, which is demonstrated in Figure 16.

As the beam gets closer to the surface these effects become evident, for example 0.03 cm from the side of the crystal there exists almost two equivalent peaks, see Figure 17. An examination of how the mean energy varies with distance to the surface was conducted, with results in Figure 18.

As seen in Figure 18 the effect occurs only when the particles get very close to the surface of the crystal. Therefore one should, when calibrating the crystal, position the scintillators in such a manner that trajectories of muons with less than 5 mm to the surface are suppressed.

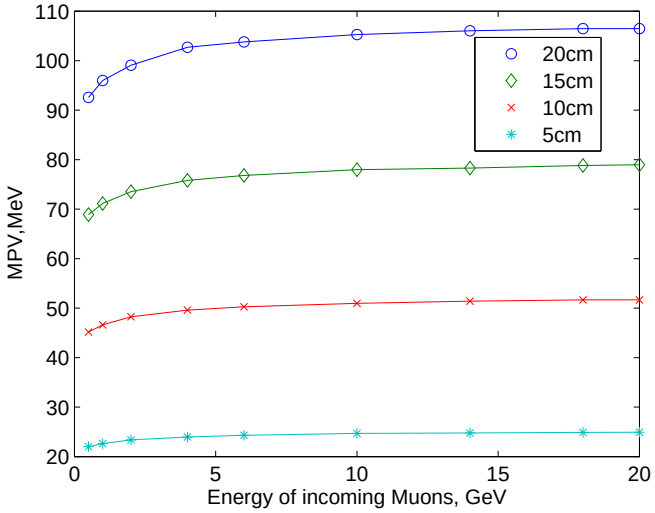

Figure 15: MPV from the Landau fit of energy deposited by muons with varying incoming energies. This was done for muons traversing four different lengths of an NaI crystal.

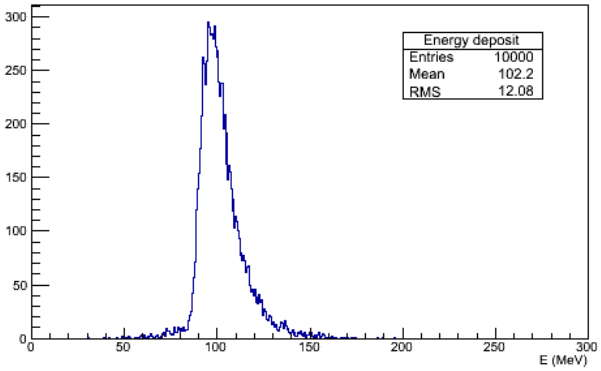

Figure 16: Deposited energy for muons hitting the NaI cylinder 0.9 cm from the edge. The cylinder's length is 20 cm.

4.2 Proton behaviour

Protons are, unlike muons, not minimum ionizing particles in the interesting energy range. Therefore one can not expect the energy deposit to behave like the energy loss experienced by muons. The histograms that result from the proton simulations were fitted with Gaussian distributions instead of Landau distributions used for muons. For sub-punchthrough energies, the histograms were not fitted with any function since the protons deposit all their energy and give rise to a well-defined peak, see Figure 19.

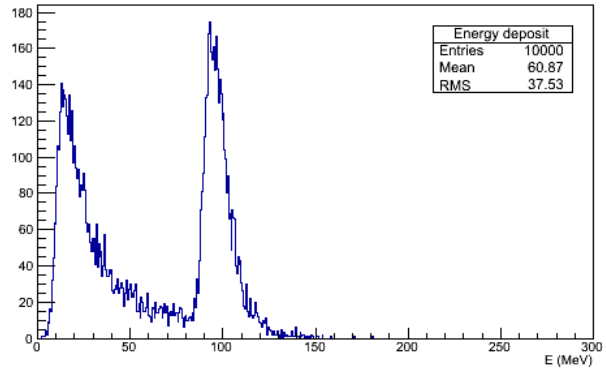

Figure 17: Energy deposited by muons impinging 0.03 cm from the surface of a 20 cm long NaI cylinder.

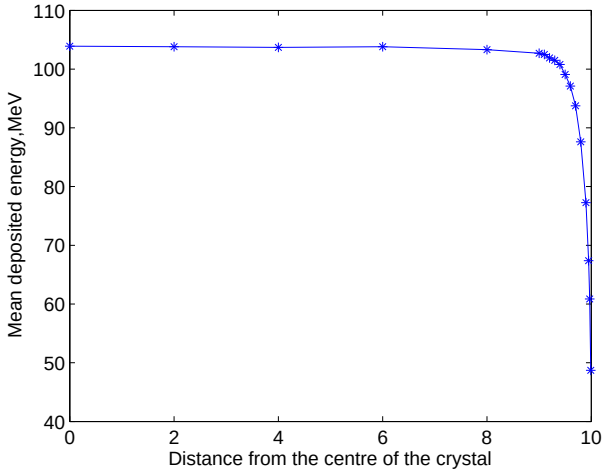

Figure 18: Surface effect illustrated by plotting the mean deposited energy of incoming muons with 1.0 GeV energy versus the distance from the centre where the muon hits the cylinder surface. The cylinder has a radius of 10 cm.

4.2.1 Punchthrough energies

To examine the behaviour of protons, they were simulated with different energies traversing through cylinders of varying length and the results can be seen in Figure 20.

Since it is helpful to visualize how the punchthrough energy varies with traversed length, the energies where punchthrough first occur is plotted against the length of the crystal, see Figure 21.

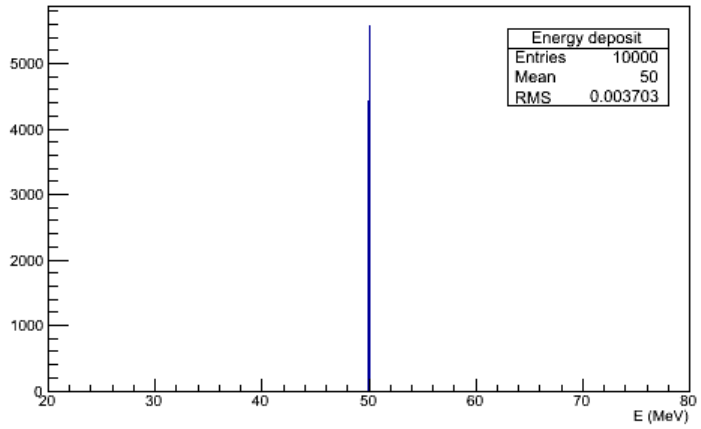

Figure 19: The energy deposited by protons with 50 MeV kinetic energy in a 10 cm long NaI crystal.

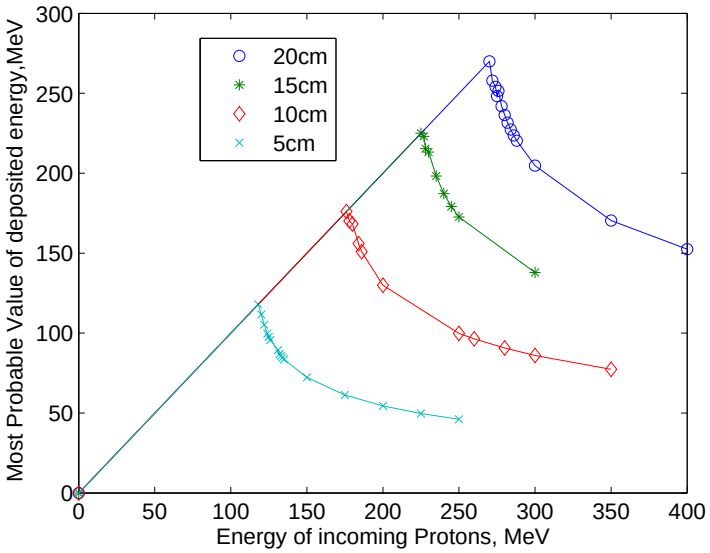

Figure 20: MPV from the Gaussian fits from simulations where protons with different energies are shot through NaI crystals of varying lengths, plotted against the incoming energy. The non-linear parts correspond to energies larger than the punchthrough energies. The plot contains error-bars (for the MPV-value) for energies above punchthrough energies which are not visible due to their small size.

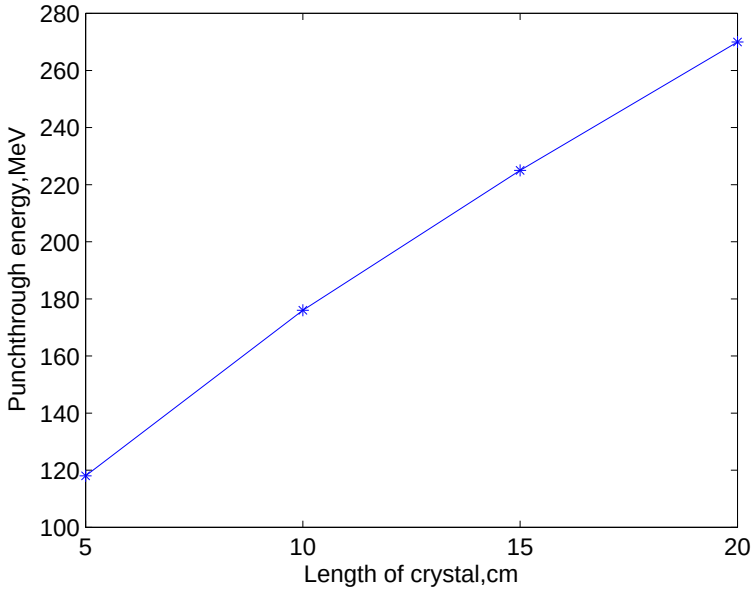

Figure 21: Punchthrough energies plotted against the length of the NaI crystal in which they are recorded. This figure does not contain error-bars.

5 Results

We will present the results obtained from simulations with horizontal scintillators, see section 3.5, in the following section and then move on to results from variations of vertical ones as described in section 3.6.

5.1 Horizontal scintillators

Results from variations in area will be presented first, followed by results from muon flux calculations and lastly results from simulations where separation was varied.

5.1.1 Variations in area

Results from simulations with differently sized scintillators are shown in Figure 22 and Table 4.

(a) $5.5 \times 5.5\,\mathrm{cm}$ (b) $9.5 \times 9.5\,\mathrm{cm}$

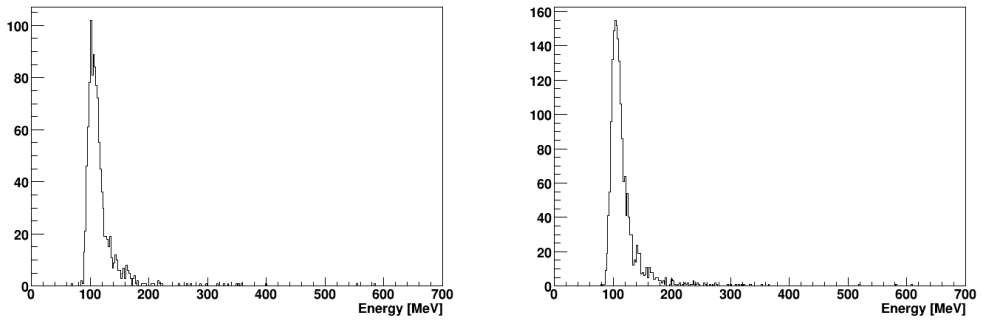

(c) $13.5 \times 13.5\,\mathrm{cm}$ (d) $17.5 \times 17.5\,\mathrm{cm}$

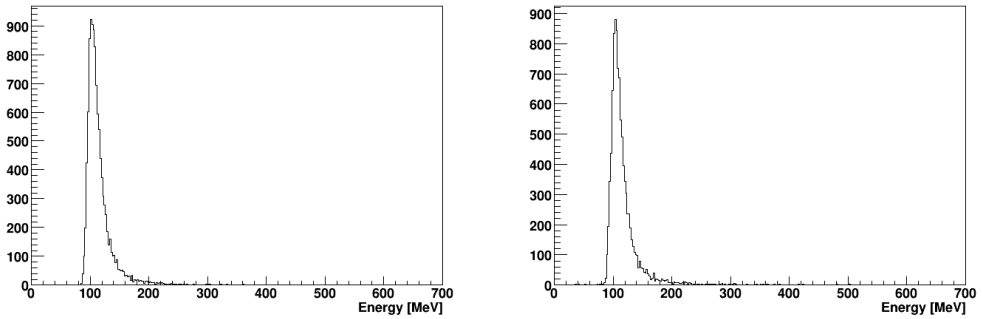

Figure 22: Histograms of energies deposited in the NaI crystal for horizontal square plastic scintillators of different side lengths. Note the different scales of the y-axis.

The data show that the variation in size hardly affects the values of MPV or σ, but that it has a significant effect on the number of muons that pass through both scintillators in a given timespan.

side [cm]	n	MPV(σ) [MeV]	hits/10^6
5.5	1121	102.74(5.09)	22.4
9.5	1861	103.04(4.88)	62.0
13.5	11079	102.57(4.67)	123.1
17.5	10020	102.54(4.71)	200.4

Table 4: Results from simulations of horizontal muons for back scintillators with different side lengths. n is the registered number of particles, MPV and σ are the "most probable value" and its corresponding uncertainity from a Landau fit to the data. Hits/10^6 is the number of muons that took a path through both scintillators per one million simulated muons.

5.1.2 Muon particle flux

The limiting factor for the calibration detector is the number of muons that pass the horizontal setup in the time allowed. The horizontal scintillator setup with the most favorable geometry has a total muon particle flux of $J_{tot} = 7.2788 \cdot 10^{-4}\,\mathrm{s}^{-1}$ i.e. one muon passes the two detectors every 1374 seconds ($\tau = 1374\,\mathrm{s}$). See Table 5 for the time required for different number of muon hits in the horizontal scintillators.

Hits	Time [days]	σ (error(σ)) [MeV]
100	1.59	10.2651 ($\pm$3.64152)
200	3.18	6.14709 ($\pm$0.555548)
750	11.93	5.28359 ($\pm$0.231295)
1250	19.88	4.60752 ($\pm$1.68733)

Table 5: Estimated time required for different numbers of muon hits in the horizontal setup, σ is the "width" of a Landau fit to the data.

5.1.3 Variations in separation

Results from the simulations where scintillator separation was varied can be seen in Figure 23 and Table 6.

separation [cm]	n	MPV(σ) [MeV]	hits/10^6
42	1330	102.42(4.70)	14.8
47	932	102.50(5.17)	11.7
52	732	102.02(4.98)	9.0
57	427	102.92(5.14)	7.12

Table 6: Results from simulations of horizontal muons for different plastic scintillator separations. n is the registered number of particles, MPV and σ are the "most probable value" and spread of a Landau fit to the data. Hits/10^6 is the number of muons that took a path through both scintillators per one million simulated (i.e. a fixed interval of time).

(a) 42 cm (b) 47 cm

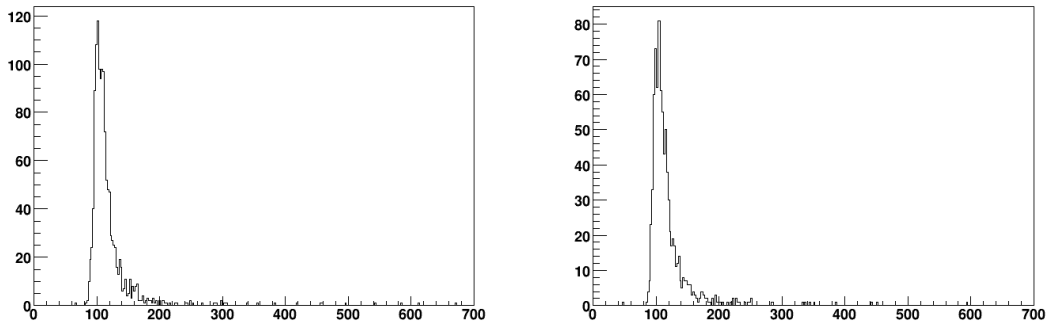

(c) 52 cm (d) 57 cm

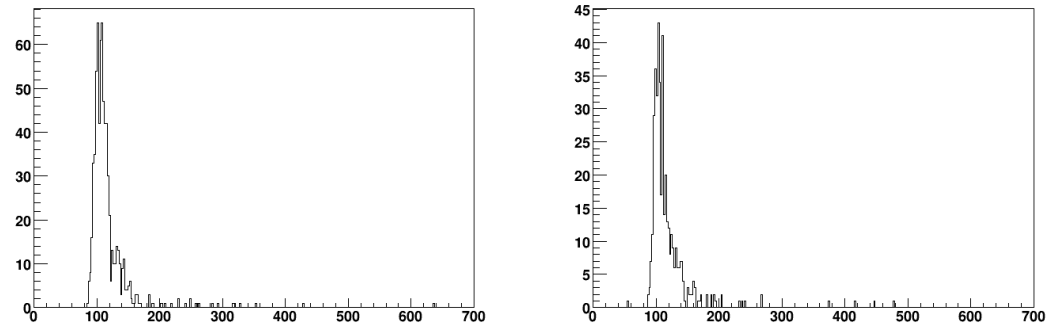

Figure 23: Histograms of energies deposited in the crystal for horizontal trajectory square scintillators of the same size, but with different separations. Note the different scales of the y-axis.

The data show that the variation in separation hardly has any effect on the values of MPV or σ, but that it has a significant effect on how many muons that pass through both scintillators in a given timespan.

5.2 Vertical scintillators

The scintillator setups can be seen in Figure 24. The scintillators were placed above and below the crystal as in Figure 10, with a separation of 15 cm. The diagrams show the MPV and σ of a Landau fit to the amount of deposited energy in the crystal when a muon passed through two scintillators aligned on top of each other. Obtained values for minimum, maximum and mean of σ can be found in Table 7.

The data show that, as the scintillators get smaller, the σ of the Landau fits get smaller, which corresponds to a narrower distribution of energy deposited in the crystal when a muon has travelled through two plastic scintillators placed vertically above each other. Data also shows that when when the scintillator size shrinks below (roughly) 5×5 cm the values of σ_{mean} and σ_{max}

Size	n	σ_{min} [MeV]	σ_{mean} [MeV]	σ_{max} [MeV]
$10 \times 20\,\text{cm}$	1	4.13	4.13	4.13
$10 \times 10\,\text{cm}$	2	2.49	2.71	2.93
$6.67 \times 6.67\,\text{cm}$	3	1.96	2.41	2.72
$5 \times 5\,\text{cm}$	4	2.01	2.46	2.83
$4 \times 4\,\text{cm}$	5	1.91	2.39	2.87
$3.33 \times 3.33\,\text{cm}$	6	1.89	2.30	2.56
$2.86 \times 2.86\,\text{cm}$	7	1.78	2.40	2.83
$2.5 \times 2.5\,\text{cm}$	8	1.76	2.40	2.94

Table 7: Results from simulations of vertical scintillator setups. Data presented as scintillator sizes, number of crystals in a scintillator array together with minimum, mean and max values of σ from a Landau fit to the data.

do not decrease any more. The fact that σ_{min} still decreases with decreased scintillator size is probably due to surface effects: as the scintillators shrink in this simulation, the outermost ones get closer to the edges and thus measure trajectories that are close to a surface, where energy gets dissipated to the outside of the detector with high probability.

This implies that there is a limit where the broadening of the deposited energy due to the size of the scintillators is negligible, and the observed broadening can be traced to the statistical physical processes of particles interacting with matter, which introduces an uncertainty in how much energy is deposited. This also means that there is a limit beyond which it is neither useful nor necessary to shrink the scintillators.

(a) $10 \times 20\,\text{cm}$ (b) Deposited energy

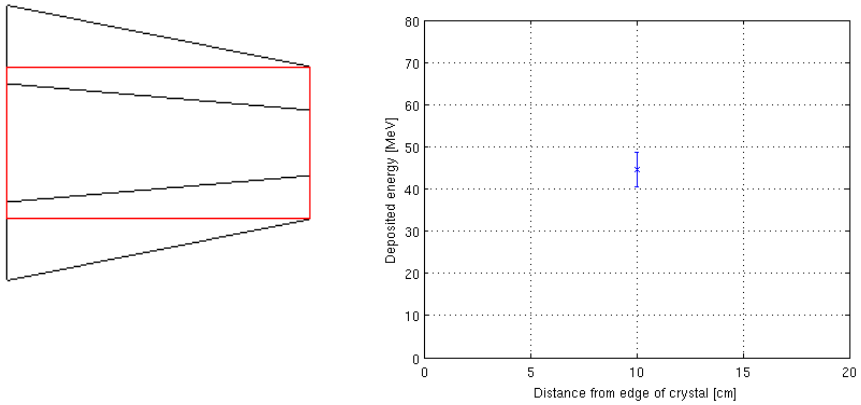

(c) $6.67 \times 6.67\,\text{cm}$ (d) Deposited energy

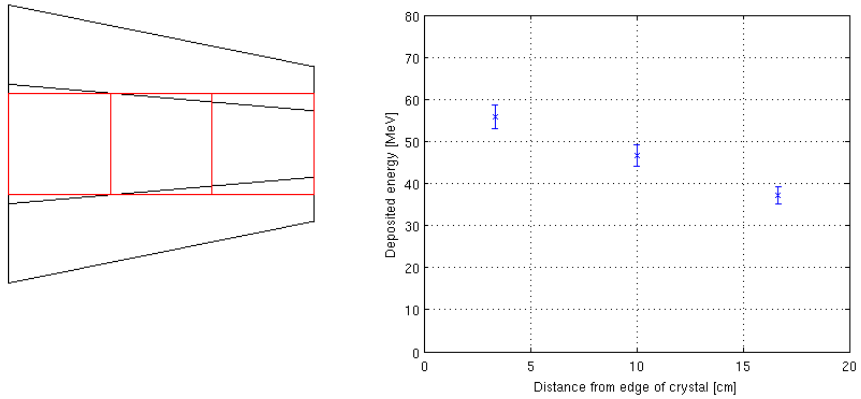

(e) $2.86 \times 2.86\,\text{cm}$ (f) Deposited energy

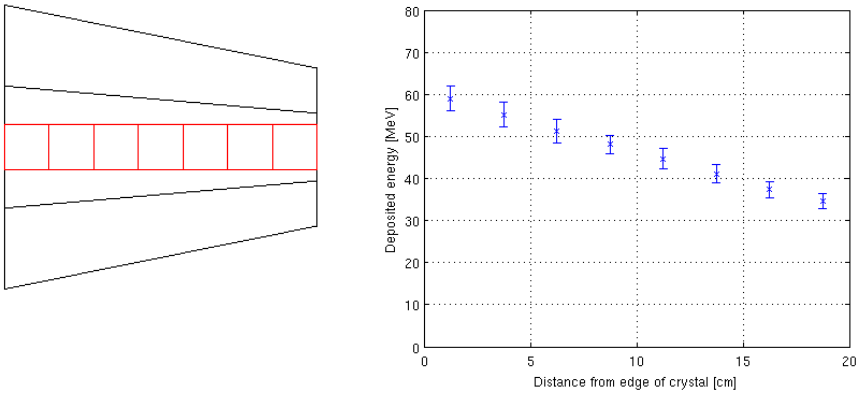

Figure 24: Scintillator sizes and setups with corresponding deposited energies. The crosses and error bars represent MPV and σ from a curve fit to a Landau distribution. The x-coordinates in the plots show the distance from the broad end of the crystal to the center of a scintillator.

6 Suggested experimental setup

We have studied two different types of setups for the calibration, one with ordinary scintillation counters and one with position sensitive scintillation counters.

The latter one is suspected to be close to impossible or at least very hard to implement with enough precision and is thereby not recommended. The idea though, from our point of view, is an elegant and interesting one and might be worth further investigation if there is time, money and interest.

6.1 Ordinary scintillation counter

The bottleneck in the process of measuring muons is, as earlier mentioned, the horizontal flux through the length of the crystal, given that the crystal should stay horizontal during the collection of data, and that the calibration should not take more time than three days.

The simulations above have shown that since the size of the back scintillator does not affect the MPV or σ, it would be preferable to maximize the areas of the horizontal scintillators, while making sure that the muons going through both scintillators traverse the whole length of the crystal. Considering the needed space for a PMT at the back end of the crystal, we suggest two square scintillators - 5×5 cm and 13.7×13.7 cm, see Figure 25.

It was also shown that shrinking the square scintillators beyond 5×5 cm did not improve much on the error of the measurement, so we suggest using scintillators of this size. In order to minimize the impact of surface effects the scintillators should be placed at least 1 cm from edges, see Figure 16. These things considered we would suggest a setup with three pairs of scintillators measuring 5×5 cm placed vertically above each other, 1 cm from the back edge of the crystal. The placement over the thicker end minimizes the relative difference between the longest and the shortest possible traversed path traversed through the crystal by the muons.

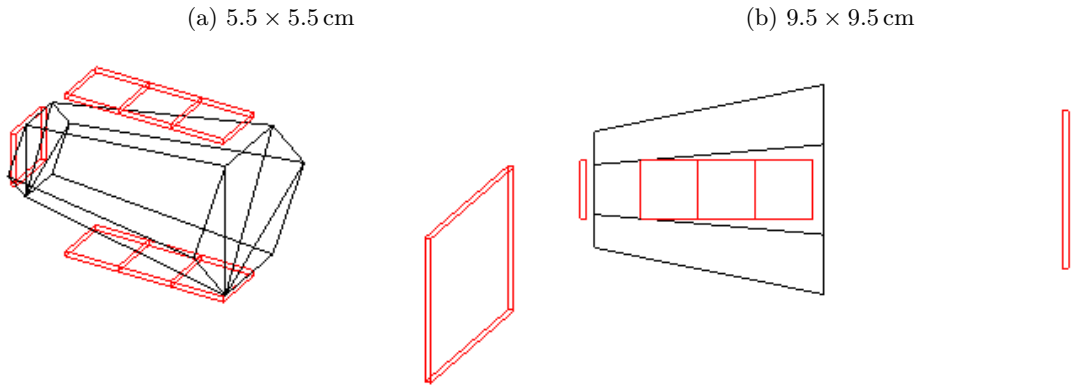

Figure 25: Scintillator setup to maximize horizontal muon flux, avoid surface effects, and gather accurate data with plastic scintillators.

6.2 Position sensitive scintillation counter

One idea that we investigated is connecting four photomultiplier tubes (PMTs) to each scintillator, thereby making it possible to calculate where muons hit the scintillator in the following way.

The equation for a circle in a Cartesian coordinate system is

$$(x-a)^2 + (y-b)^2 = r^2 \tag{19}$$

where (a, b) is the center and r is the radius.

When a muon travels through the scintillator photons are emitted. Part of these photons are then detected by the PMTs. If the scintillator is thin, one can assume that it is two dimensional which means that the muon travels through it at a position (x_m,y_m), see Figure 26.

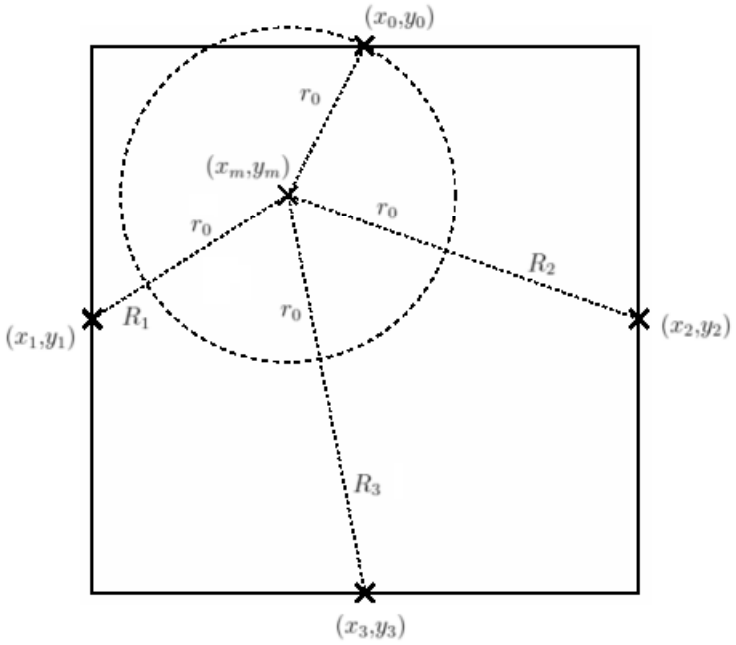

Figure 26: An example of a muon passing the position sensitive scintillator at (x_m,y_m).

From Figure 26 one sees that the connection points for the PMTs are located on circles centered at (x_m, y_m) and with radii r_0, $(R_1 + r_0)$, $(R_2 + r_0)$ and $(R_3 + r_0)$, respectively. To get R_1, R_2 and R_3 one multiplies the time difference measured between each connection point and the connection point for the PMT which is first to detect photons. In reality one will have to know the time it takes for photons to travel between a connection point a PMT so one can substract that time from the actual measured time.

If one inserts the radius and position for the connection points into the equation for a circle (19) one gets four coupled equations (20).

$$\begin{cases} x_0^2 - 2x_0x_m + x_m^2 + y_0^2 - 2y_0y_m + y_m^2 = r_0^2 \\ x_i^2 - 2x_ix_m + x_m^2 + y_i^2 - 2y_iy_m + y_m^2 = r_0^2 + r_0R_i + R_i^2 \qquad i = 1,2,3 \end{cases} \tag{20}$$

Substitution of the first equation from the three others and some algebra results in a matrix equation (21).

$$\begin{bmatrix} 2x_0 - 2x_1 & 2y_0 - 2y_1 & -R_1 \\ 2x_0 - 2x_2 & 2y_0 - 2y_2 & -R_2 \\ 2x_0 - 2x_3 & 2y_0 - 2y_3 & -R_3 \end{bmatrix} \begin{bmatrix} x_m \\ y_m \\ r_0 \end{bmatrix} = \begin{bmatrix} x_0^2 - x_1^2 + y_0^2 - y_1^2 + R_1^2 \\ x_0^2 - x_2^2 + y_0^2 - y_2^2 + R_2^2 \\ x_0^2 - x_3^2 + y_0^2 - y_3^2 + R_3^2 \end{bmatrix} \tag{21}$$

Solving this system of equations gives (x_m, y_m) which is the point where the muon passed the scintillator.

Using this setup one could theoretically just place one big scintillator above and one below the crystal and then be able to trace most of the muons traversing the crystal. This makes it possible to obtain a huge amount of data in a short time even though one might have to throw away some undesirable data due to the scintillators being so large compared to the crystal.

7 Conclusions and Discussion

To calibrate a single crystal with the proton beam, we note that the beam has a well-defined energy and this energy should be such that it is below the punchthrough energy. This can be guaranteed thanks to the fact that the punchthrough energy varies linearly with length, see Figure 21. The path that the proton beam will take is 20 cm long and the proton energy should thus be less than 288 MeV.

This beam, which is monodirectional and monoenergetic, gives us a well-defined peak in the deposited energy corresponding to the incoming energy of the protons, see Figure 19. The resolution, being less than 2 % for protons being stopped in the crystal [21], will not affect the results. The energy deposited in the crystal by incoming protons will be known by correlating the signal resulting from muon interactions in the crystal and the deposited energy of the protons.

From the simulations in section 4.1.1 one sees that muons in this energy-range do indeed behave as minimum ionizing particles. As such, the deposited energy should not depend on the incoming energy of the muons, which is supported by our simulations, see Figure 14. One can thus use muons to calibrate the Crystal Ball. Their path through the detector array is known because single muons will make different crystals "fire off" in coincidence, making it possible to calculate the path traversed. The signal resulting from the energy deposit can hence be calibrated.

An issue that arises for protons that are not stopped by Crystal Ball is that their energy can not be determined unambiguously. There is therefore a risk of them being mistaken for lower energy stopped ones, see Figure 20.

One thing that should be considered in further studies and simulations is how the thickness of the plastic scintillators affects the processes. This study only considered square plastic scintillators with a fixed thickness of 0.5 cm. It would be of interest to run more simulations with other shapes and thicknesses to further investigate parameters that would contribute to making good measurements. Geant4 has many possibilities to easily simulate physical bodies of many different geometrical shapes, and plastic can be manufactured into many different shapes, so the realizable variations are endless in both simulations and in the lab.

Simulations were time consuming with the computer power available to the group. The simulation time required to get a decent amount of muons through both scintillators in the horizontal setups could take up to 10 hours for small scintillator sizes. One should look into possibilities to optimize the code, especially the muon distribution, to speed up simulations, and make time available for testing more scintillator setups and properties.

There has been some indications that the theoretical muon distribution might have too low intensity for muons at angles close to the horizon. Researchers have found that experiments yielded a horizontal muon flux about twice as large as the simulations predict [20]. This is promising, as it would cut down calibration time by half.

References

[1] Adrich, P. (2003) *The Crystal Ball γ-Detector Setup and Calibration*. Retrieved 8 February, 2012, from GSI Helmholtzzentrum für Schwerionenforschung GmbH.
`http://www.gsi.de/forschung/kp/kp2/collaborations/land/doc/detectors/crystal_ball/cb_docu.pdf`

[2] Geant4 collaboration, Agostinelli, S. et al. (2003). Geant 4 - a simulation toolkit, *Nuclear Instrument and Methods in Physics Research A*, vol. 506, pp. 250-303.

[3] Geant4 collaboration, Allison, J. et al. (2006). Geant4 developments and applications, *IEEE Transactions on Nuclear Science*, vol. 53, pp. 270-278.

[4] Amako, K. et al. (2005). Comparison of Geant4 electromagnetic physics models against the NIST reference data, *IEE Transactions on Nuclear Science*, vol. 52, pp. 910-918.

[5] Cirrone, G.A.P. et al. (2004). Precision validation of Geant4 electromagnetic physics, *i Conf. Rec. 2003 IEEE Nuclear Science Symposium*, vol. N23-2.

[6] Leo, W. R., (1994) *Techniques for Nuclear and Particle Physics Experiments*. Second revised edition. Berlin Heidelberg: Springer-Verlag.

[7] Devons, s et al. (1960). *Muon Mass and Charge by Critical Absorption of Mesonic X Rays*. Retrieved 15 May, 2012, from Columbia University.
`http://prl.aps.org/pdf/PRL/v5/i7/p330_1`

[8] Green, D. (2000). Ionization. In *The Physics of Particle Detectors*, red. D. Green, ss. 107-108. Cambridge: Cambridge University Press.

[9] Groom, D E. Klein, S R. (1999). *Passage of particles through matter*. Retrieved 10 May, 2012, from Lawrence Berkeley National Laboratory.
`http://www.springerlink.com/content/m321677145684107/fulltext.pdf`

[10] Groom, D E. Mokhov, N V. Striganov, S I. (2001) Muon Stopping Power and Range Tables 10 MeV-100 MeV. *Atomic Data and Nuclear Data Tables*, vol. 76, nr 2, pp. 183-356.
`http://pdg.lbl.gov/2008/AtomicNuclearProperties/adndt.pdf`

[11] Private communication with Heinz, A M. 15 May, 2012, from Chalmers University of Technology.

[12] Kempa, J. Brancus, M. (2003). Zenith angle distributions of cosmic ray muons. *Nuclear Physics B (Proc. Suppl.)*, vol. 122, pp. 279-281.

[13] Kempa, J. Krawczynska, A. (2006). *Low energy muons in the cosmic radiation*. Retrieved 13 Mars, 2012, from Warzaw University of Technology.

[14] Liu, L. (2007). *The Speed and Lifetime of Cosmic Ray Muons*. Retrieved 15 May, 2012, from Massachusetts Institute of Technology.
`http://web.mit.edu/lululiu/Public/pixx/not-pixx/muons.pdf`

[15] National University of La Plata. (n. d.). *Muon basics*. Retrieved 8 February, 2012, from National University of La Plata.
`http://www.fisica.unlp.edu.ar/~veiga/experiments.html`

[16] Nilsson, T. (2011). *ROOT analysis, simple simulation and curve fitting write-up for the course "FUF065/FIM465 Advanced Subatomic Detection and Analysis Methods"*. Retrieved 9 February, 2012, from Chalmers University of Technology.
`http://fy.chalmers.se/subatom/advsubdet/ROOT_small.pdf`

[17] Official website of the Geant4 collaboration. (n. d.). *Geant4: A toolkit for the simulation of the passage of particles through matter*. Retrieved 9 February, 2012, from
`http://geant4.org/`

[18] *ROOT*, Retrieved 15 May, 2012, from `http://root.cern.ch/`

[19] Saint-Gobain Ceramics & Plastics Inc. (2005). *BC-400, BC-404, BC-408, BC-412, BC-416 Premium Plastic Scintillators Datasheet*.

[20] Private communication with Thies, R. 15 May, 2012, from Chalmers University of Technology.

[21] Wamers, F. (2011). *Quasi-Free-Scattering and One-Proton-Removal Reactions with the Proton-Dripline Nucleus ^{17}Ne at Relativistic Beam Energies*, Technische Universität Darmstadt, pp. 31-32.